Polymer-based Nanocomposites of P(VDF-TrFE)/Bi$_2$O$_3$ Applied to X-ray Shielding

Fontainha CCP[1], Baptista-Neto AT[2] and Faria LO[2]*

[1]Department. Nuclear Engineering, Federal University of Minas Gerais.- UFMG, Av Antônio Carlos, 6627, CEP 31270-970, Belo Horizonte, MG, Brazil

[2]Nuclear Technology Development Center- CDTN, Av Antônio Carlos 6627, C.P. 941, CEP 31270-901, Belo Horizonte, MG, Brazil

Research Article

ABSTRACT

Radiology procedures such as fluoroscopy provide high doses to patients because they involve long periods of direct X-rays beam pointing to the same region. Composite materials containing compounds or elements with good attenuation properties such as barium sulfate and lead have been studied elsewhere. In this study, polymer based composites made of Poly(vinylidene fluoride-tryfluorethylene) [P(VDF-TrFE)] copolymers and micro and nanosized crystalline Bismuth Oxide were prepared. The main objective of this work was to identify the morphological differences between micro and nanocomposites and their performance as X-ray shielding material. The bismuth oxide was previously surface-modified with Methyl-Methacrylate Acid (MMA) in order to improve the homogeneity distribution. The X-ray shielding characterization was performed for photons with energies ranging from 6.5 keV to 83.5 keV. The nanocomposite P(VDF-TrFE)/nano Bi$_2$O$_3$-MMA revealed to have better attenuation features than the microcomposite, in the entire range of energy studied. DRX, DSC, FTIR and SEM images data were used in order to understand the difference in the radiation shielding features. The investigation has demonstrated that the P(VDF-TrFE)/nano Bi$_2$O$_3$-MMA nanocomposites are good candidates for application in radiology procedures as lightweight, conformable, flexible, and easy to process X-ray shielding materials.

INTRODUCTION

Exposures to high-energy or ionizing radiation can be hazardous to health. Radiation doses from either particle-emissions or high-energy electromagnetic waves such as X-rays/γ rays, may result in carcinogenesis, cell mutations and organ failure. Interventional radiology procedures such as fluoroscopy provide high doses to patients because they involve long periods of direct X-rays beam pointing to the same region. Digital mammography and radiography also provide radiation doses to the skin above the established limits [1,2]. Thus, nowadays, there is a great interest in developing new radiation attenuator composites that shield part of the X-ray incident beam, aiming to minimize the patient skin injuries in specific high dose radiology procedures.

Polymeric compounds are lightweight, conformable, flexible, and easy to process materials. Due to these properties, polymeric based mixtures are ideal candidates to produce thin and lightweight composites required in a wide range of technological applications. Polymer-composite materials for radiation protection filled with compounds or elements with good attenuation properties such as barium sulfate, gadolinium, lead, molybdenum, rhodium, tungsten, bismuth, zirconium oxide and iron oxide have been studied elsewhere [3]. According to Nambiar and Yeow [3], polymers reinforced with micro- or nanoscale structures have

great potential to be used as radiation shielding materials also in all medical radiology applications. Moreover, the general trend seems to be toward development of novel, multifunctional polymer nanocomposites exploiting the properties of nanofillers. In recent years, few groups have explored the radiation-resistant properties of polymer nanocomposites [4,5]. In this context, both experimental and simulation studies reported that nanocrystalline materials showed enhanced radiation-resistance when compared to their macrocrystalline counterparts. This property of nanomaterials has been attributed to the large volume fraction of grain boundaries that may serve as effective sinks for defects produced upon irradiation of ionizing radiation [6-8]. Few studies have proposed the use of nanocomposites of a high-performance polymer - polybenzimidazole and carbon nanofibers or other nano-materials for durable space applications [9,10]. Carbon-based filler materials such as carbon micro/nanofibers and also nanotubes have been used as reinforcements in a variety of polymers (resins and plastics), exhibiting high strength-to-weight ratio. Gaier et al. [11] demonstrated the application of graphite microfiber-based epoxy resin composites for shielding against cosmic radiation.

On the other hand, conventional-sized Bismuth Oxide has been reported by Hopper et al. [12] to be used in a bismuth-coated latex shields (340 g/cm^2) for breast radiography. This material saved an average 57% of the radiation dose to the breast from thoracic CT, decreasing the radiation level from an average 22 mGy to 10 mGy. Fricke et al. [13], using the same bismuth-coated latex but with 170 g/cm^2 of bismuth and constructed with a 1-cm foam pad placed between the bismuth latex and the patient, reported 29% reduction in radiation dose without any perceptible change in image quality. On the other hand, the incorporation of Bismuth Oxide nanoparticles into surface coatings, polymer composites, and textiles can provide protection from harmful x-ray radiation without significantly impacting mechanical properties. This type of protection has remained a long-standing challenge since the use of conventional-sized fillers for x-ray attenuation may significantly degrade the mechanical integrity of polymers. In this context, Nambiar et al. [14] reported that Polydimethylsiloxane [PDMS] nanocomposites were filled with 44.44 wt% of bismuth oxide (BO) nanopowder. This nanocomposite (3.73-mm thick) was capable of attenuating all the scattered X-rays generated at a tube potential of 60 kV.

Poly(vinylidene fluoride) [PVDF] and PVDF-based copolymers/blends have been investigated as potential components in dielectric nanocomposite materials for high energy density capacitor applications [15]. It includes various fields such as optoelectronics and temperature and vapor/liquid sensing [16,17]. In an early recent work we have proposed a crystalline nanocomposite made of Poly(Vinylidene Fluoride-Tryfluorethylene) [P(VDF-TrFE)] copolymer and Methyl Methacrylate [MMA] surface-modified ZrO_2 nanoparticles, for application in X-ray shielding [18]. In that nanocomposite, the compatibility between P(VDF-TrFE) and MMA [19] played a crucial role in order to provide a much better homogeneous distribution of ZrO_2 nanoparticles into the polymeric matrix. In this work we investigate the radiation shielding properties of composites made of semi-crystalline P(VDF-TrFE) copolymers filled with crystalline Bi_2O_3 particles. We aim to identify the morphological differences between micro and nanocomposites by using micro and nanoparticles of crystalline Bi_2O_3 and their respective performance as X-ray shielding material. In an attempt to take advantage of the miscibility between P(VDF-TrFE) and MMA in favor of a better homogeneous distribution of nano- and microsized Bi_2O_3 particulate in the P(VDF-TrFE) matrix, the filler material was mixed with MMA in a first step. In a second step, the MMA/Bi_2O_3 mixture was mixed with the P(VDF-TrFE) copolymer. Following this methodology, P(VDF-TrFE)/nanocrystalline Bi_2O_3 and also P(VDF-TrFE)/microcrystalline Bi_2O_3 composites were produced. The radiation shielding characterization was performed using mono-energetic X-rays with energies of 6.5 keV, 17.5 keV and 22.1 keV and also for non-monochromatic fields with mean energies of 33 keV, 54 keV and 83 keV. The X-ray shielding properties of both composites are discussed and explained in terms of chemical and morphological differences between them.

MATERIALS AND METHODS

P(VDF–TrFE) copolymers resins with 50% of TrFE contents were supplied by ATOCHEM (France). Microsized or nanosized Bismuth Oxide particles and MMA were mixed together and were prepared by dissolving in a solvent formed by n,n–dimethylacetamide (DMAc) and 1% Acetic Anhydride at 60°C, in a 10:1 concentration. The solution containing the surface-modified Bi_2O_3 were then stirred during 30 min at 60°C and casted with a solution containing P(VDF-TrFE) copolymers also dissolved at DMAc and 1% Acetic Anhydride. The amount of micro or nanoparticles Bi_2O_3 in the composite was always 8.0 wt%. The solution containing the P(VDF-TrFE)/Bi_2O_3-MMA composites were then stirred again during 30 min at 60°C and placed in an oven in order to evaporate. Films of c.a. 70 µm were produced using this methodology.

Composite characterization

Composite characterization was performed with Field-emission electron microscopy (FE-SEM), Energy Dispersive X-ray Spectrometry (EDS), Differential Scanning Calorimetry (DSC), X-ray diffraction (XRD) and infrared spectroscopy (FTIR) techniques. The FTIR spectra were collected by a BOMEM 100 spectrometer in the Transmission mode by putting the films directly exposed to the FTIR beam, for wavenumbers ranging from 200 to 4,000 cm^{-1}. The beam was always focused in the center of each c.a. 70 µm film sample. By using this methodology we assume that the quantities of Bi_2O_3 were in principle homogeneously distributed inside the polymeric matrix. Thermal behavior studies were made by using a DSC TA Q10, with heating and cooling rates of 10°C/min, in the second run, from 25 to 200°C. Typical sample weight was 10 mg. Structural characterization was made by x-ray diffractometry (RIGAKU), with a 2° 2θ/min scan rate, using CuK_α radiation (30 mA, 40 kV). FE-SEM microscopy were performed at a SIGMA VP

field emission scanning electron microscope ZEISS. The EDS spectrometry was performed by using a Bruker Nano GmbH, Model XFlash Detector 410-M, coupled to the SEM system.

Radiation shielding characterization

For lower photon energies ranging from 6.5 keV to 22.1 keV, the radiation shielding characterization was performed using an incident monochromatic X-ray beam from the RIGAKU diffractometer. **Figure 1** depicts a diagram explaining the irradiation setup. In order to generate a monochromatic incident X-ray beam, a non-monochromatic X-ray was first directed to a single crystal of Si(111). The constructive diffraction from the CoK_α, (E=6.5 keV), MoK_α, (E=17.5 keV) and AgK_α,(E=22.1 keV) X-ray beams were obtained at 2θ approximately equal to 33.13°, 12.96° and 10.25°, respectively.
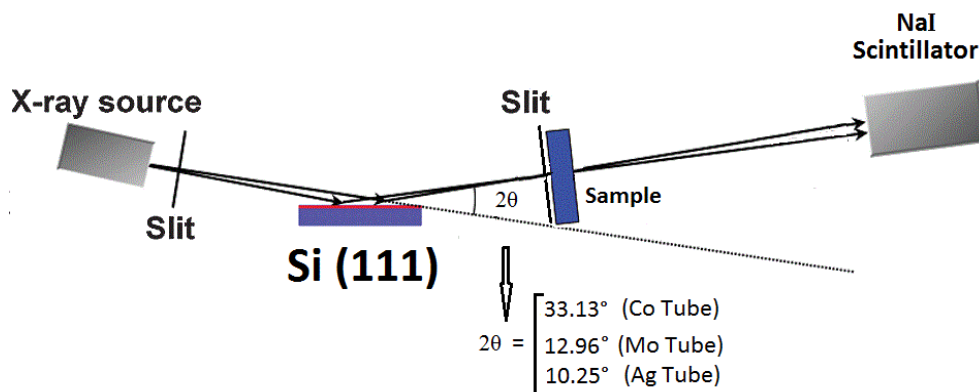
Figure 1: Schematic diagram of the setup used to irradiate P(VDF-TrFE)/Bi_2O_3 samples with monoenergetic X-rays using Co, Mo and Ag tubes with photons of 6.5 keV, 17,5 keV and 22,1 keV, respectively.

For higher photon energies, samples were irradiated non monochromatic fields at the same dose (100 mGy) for the X-ray beam qualities RQR2 (40kV), RQR5 (70 kV) and RQR 8 (100 kV), as shown in **Table 1**. Tests were carried out using a Pantak Seifert Model 320 HS x-ray machine and the same setup was adopted for all samples under comparison. This device's inherent filtration was estimated at 0.18 mm Al by means of the extrapolation method described in ISO 4037-1.

Table 1: Main parameters of the Radiation Qualities used to irradiate P(VDF-TrFE)/Bi_2O_3 samples with non-monochromatic X-radiation according to ISO 4037-1.

Radiation Quality Pattern	X-ray Tube Voltage (kV)	1st HVL (mm Al)	Homogeneity coefficient
RQR2	40	1,42	0,81
RQR5	70	2,58	0,71
RQR8	100	3,97	0,68

The attenuated X-ray dose was evaluated using XR-QA2 Gafchromic® radio-chromic films, previously calibrated at RQR8 (70 kV) beam quality. The XR-QA2 films were irradiated with 100 mGy, using the setup for "Narrow series" defined by ISO 1996, in order to determine their energetic dependence. The Correction Factors, normalized to the N40 beam, and the respective mean energies are shown in **Table 2**. It is seen that, for tube voltages ranging from 40 kV to 100 kV, the correction factors are very close to one.

Table 2: Narrow spectrum series defined by ISO 1996 used to determine the energetic dependence of XR-QA2 radiochromic films. These dosimeters were used to evaluate the attenuated X-ray doses under the P(VDF-TrFE)/Bi_2O_3 samples.

Radiation Quality	Mean Energy (keV)	Correction Factor	Standard Deviation
N30	24	2,19	0,09
N40	33	1,00	0,04
N60	48	0,96	0,04
N80	65	1,03	0,04
N100	83	1,06	0,04
N120	100	1,85	0,07

RESULTS

In **Figure 2** we show two photographs taken just after the complete evaporation of P(VDF-TrFE)/Bi_2O_3-MMA solution pre-

pared with 8 wt% of Bi_2O_3 microparticles **(Figure 2a)** and nanoparticles **(Figure 2b)**. In both samples it is possible to observe that there are no visible particle clusters, which means that the presence of MMA, at least at a macroscopic level, favors a good homogeneous distribution of Bi_2O_3 microsized particles into the polymeric matrix. We remark that in a previous work [18], when investigating a similar composite made of P(VDF-TrFE) and microsized ZrO_2 particles, the composites made without the presence of MMA presented visible ZrO_2 clusters. On the other hand, another observable characteristic in **Figure 1** is concerned to color and opacity. Composite made with microsized Bi_2O_3 is translucent and that made with nanosized one is yellow and somehow opaque.
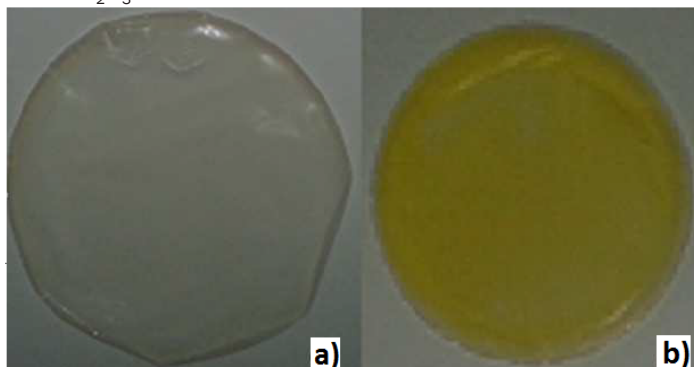
Figure 2: Photographs taken just after the complete evaporation of a typical P(VDF-TrFE)/Bi_2O_3 film sample prepared with a) 8 wt% of Bi_2O_3 microparticles and b) 8 wt% of Bi_2O_3 nanoparticles.

In **Figure 3** we present the SEM images of pristine P(VDF-TrFE) and P(VDF-TrFE)/Bi_2O_3 composites. Comparing the SEM images with lower magnification, i.e. **Figure 3a, 3b** right and **3c** right, it is seen that the surfaces of P(VDF-TrFE) copolymers and the nanocomposite are similar concerning to the apparent porosity. However, the image of the microcomposite shows a high degree of porosity, which is an unwanted feature in radiation shielding materials.
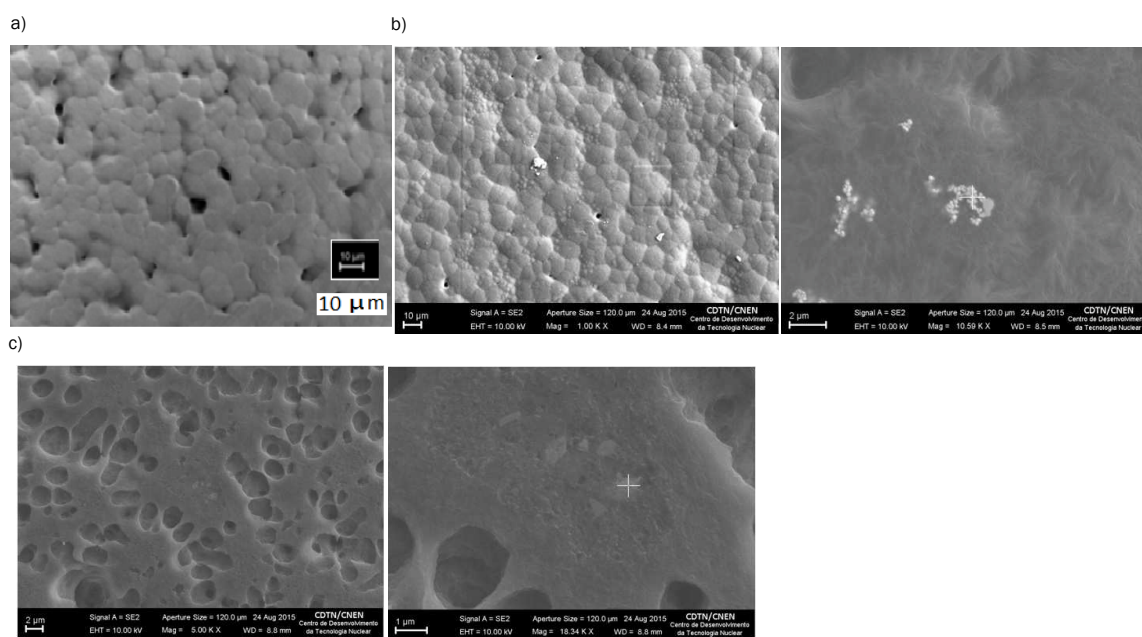
Figure 3: (a) SEM images taken on the surface of P(VDF-TrFE) pristine sample magnified 1310x (b) P(VDF-TrFE)/Bi_2O_3 nanocomposite magnified 1000x (left side) and 1050x (right side) and (c) P(VDF-TrFE)/Bi_2O_3 microcomposite magnified 5000x (left side) and 1834x (right side). The white cross mark on images [(b) and (c) left] correspond to the points where the EDS probe was pointed in order to measure the presence of Bi_2O_3 material.

In order to confirm the presence of Bi_2O_3 material in the composites, we have used the Energy Dispersive X-ray Spectrometry coupled to the SEM microscope. In **Table 3** we show the results obtained with the EDS probe pointed do the white cross position in **Figure 3a and 3b,** left side. The normalized amounts (wt.%) of Bismuth in both nano and micro composites are 36.94 wt.% and 42.76 wt.%, respectively. We remind that the initial amount of Bi_2O_3 material in the sample preparation was 8.0 wt.%. The higher values measured by the EDS probe are due to the fact the probe is pointed to nano and micro clusters of Bi_2O_3 particles, which significantly change the relative amount of Bismuth atoms. In fact, the values shown in **Table 3** just confirm that Bi_2O_3 particles are present in those clusters.

Figure 4a displays diffractograms of nano and micro crystalline Bi_2O_3. The main peaks at 27.44 and 28.08 2θ-degrees correspond to the (012) Bragg peaks of nano and microsized material, respectively. **Figure 4b** displays diffractograms of pristine P(VDF-TrFE) copolymer and its composites with nano and microsized Bi_2O_3. In the diffractograms of pristine P(VDF-TrFE), the main

Table 3: Normalized amounts (wt.%) of C, F, Bi, Au and O atoms in the P(VDF-TrFE)/Bi$_2$O$_3$ composites evaluated by Energy Dispersive X-ray Spectrometry coupled to the SEM microscope.

Element	P(VDF-TrFE)/Bi$_2$O$_3$ nanocomposite (wt.%)	P(VDF-TrFE)/Bi$_2$O$_3$ microcomposite (wt.%)
Carbon	31,52	30,32
Fluorine	24,87	22,29
Bismuth	36,94	43,76
Gold	5,44	1,32
Oxygen	1,23	2,3

peaks at 19.16, 19.60, and around 40 2θ-degrees correspond, respectively, to the (200), (110),and (201) Bragg peaks. This is the typical profile for the quasihexagonal *Cm2m* structure, also called the β-phase [20]. By comparing **Figure 4a and 4b** it is possible to verify that the P(VDF-TrFE)/Bi$_2$O$_3$ nanocomposite keeps its crystalline structure inside the composite while the diffractograms of P(VDF-TrFE)/Bi$_2$O$_3$ microcomposite reveals that the microsized Bi$_2$O$_3$ peaks are not present in this sample. In this diffractogram, only the three crystalline peaks of pristine P(VDF-TrFE) copolymer are visible.
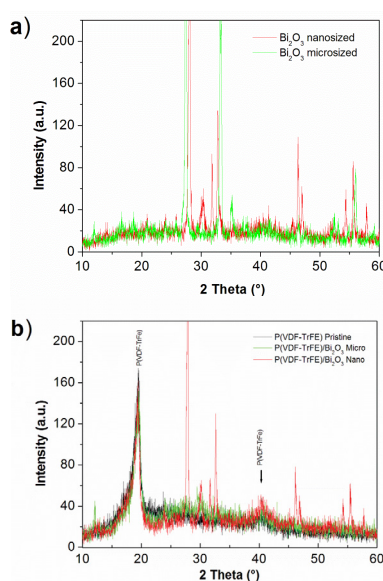

Figure 4: a) Diffractograms of nano and micro crystalline Bismuth Oxide and b) diffractograms of pristine P(VDF-TrFE) copolymer and its composites with nano and microsized Bi$_2$O$_3$.

The lack of the microsized Bi$_2$O$_3$ crystalline peaks in the P(VDF-TrFE)/Bi$_2$O$_3$ microcomposite diffractogram suggests that during the synthesis process some kind of chemical reaction must have broken the microsized Bi$_2$O$_3$ crystalline arrangement. In this context, we have performed differential scanning calorimetry in order to obtain more information concerning the composite crystalline structure such as crystalline volume melting latent heat and temperature. Heating and cooling DSC thermograms of pristine P(VDF-TrFE) copolymers and the nano and microcomposites, collected at the 2nd run, are shown in **Figure 5**. In the thermogram of pristine P(VDF-TrFE), during the heating run, there are two endothermic peaks corresponding to the ferro-to-paraelectric transition (lower temperature), called the Curie transition, and to the melting phase transitions (higher temperature) of the copolymer, respectively. On cooling, it is observed the exothermic peaks associated with the crystallization process (higher temperature) and the para-to-ferroelectric phase transition (lower temperature). These two phase transitions are reversible and show thermal hysteresis. The thermograms of the composite samples reveal that these phase transitions still occur after the synthesis process. However, the melting and crystallization transitions occur at lower temperatures and the melt latent heat (L$_M$ and L$_{Curie}$) involved in all transitions are lower than the one involved in pristine copolymer.

The calculated L$_M$ and L$_{Curie}$ values involved in the melting and Curie phase transitions and also their correspondent temperatures are given in **Table 4**. We remark that in crystalline polymers such as P(VDF-TrFE), melting happens when the polymer chains fall out of their crystal structures, and become a disordered liquid. The latent heat used to undergo the melting transition is associated with the crystalline volume. The L$_M$ values in **Table 4,** i.e. 22.64 J/g for the nanocomposite and 19.92 J/g for the microcomposite, tell us that inside the nanocomposite, the P(VDF-TrFE) crystallites has a larger crystalline volume than in the microcomposite. However, the latent heat necessary to undergo the ferro-to-paraelectric transition is the same for both composites. The composite melting temperatures are also decreased, when compared to the T$_M$ of P(VDF-TrFE) copolymer. In the same way, the T$_{Curie}$ is not affected. Summarizing, the addition of 8.0 wt.% of micro or nanosized Bi$_2$O$_3$ particles into the polymeric matrix provokes a decrease of 11% (nano) and 22% (micro) in the P(VDF-TrFE) crystalline volume, without affecting the electric dipolar interaction between the C-F dipoles in the crystallites.

Table 4: Latent heat of melting (L_M) and ferro-to-paraelectric (L_{Curie}) transitions and their respective temperatures (T_M and T_{Curie}) for the thermograms shown in **Figure 5**.

	Melting Latent Heat (J/g)	F-P Transiton Latent Heat (J/g)	Melting Temperature (°C)	F-P Transition Temperature (°C)
P(VDF-TrFE) pristine	25,38	5,136	157,5	63,5
P(VDF-TrFE)/Bi$_2$O$_3$ nanosized	22,64	4,174	155,2	63,9
P(VDF-TrFE)/Bi$_2$O$_3$ microsized	19,92	4,284	154,9	63,8
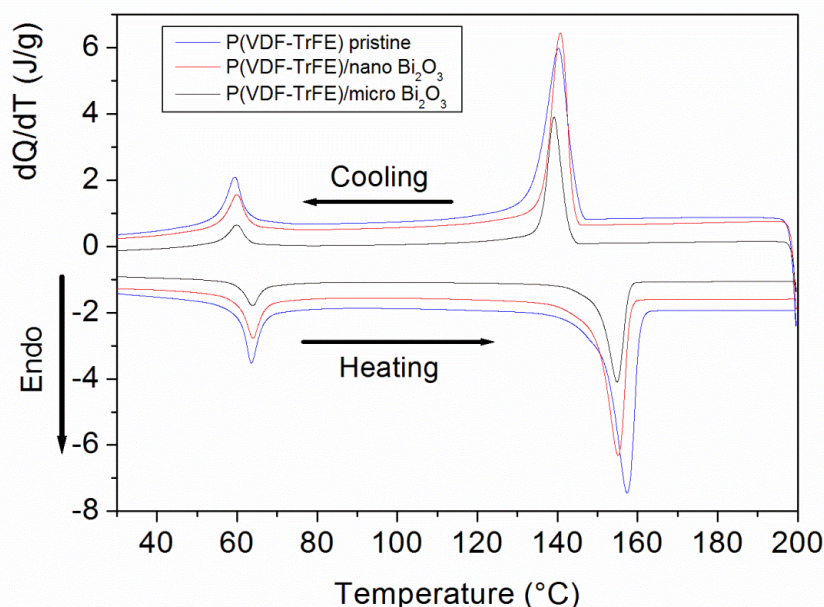
Figure 5: DSC thermograms of P(VDF-TrFE) copolymer and of P(VDF-TrFE)/Bi$_2$O$_3$ nano and microcomposites, collected at the 2nd heating/cooling run.

Figure 6 displays the FTIR spectra, ranging from 1400 cm^{-1} to 1800 cm^{-1} for pristine P(VDF-TrFE) copolymers and the nano and microcomposites. The spectrum of the P(VDF-TrFE)/Bi$_2$O$_3$ microcomposite reveals the presence of a wide and large absorption band centered at 1530 cm^{-1} and also an absorption band at 1640 cm^{-1} with lower intensity. The band at 1530 cm^{-1} is also present in the P(VDF-TrFE)/Bi$_2$O$_3$ nanocomposite, but with a significant decrease on its intensity. This band is not present in the P(VDF-TrFE) spectrum. These absorption bands suggests the presence of DMAc in the sample once they can be associated to the C=O stretch (1635-1655 cm^{-1}) and to the CH$_3$ antisymmetric deformation (1440-1470 cm^{-1}) molecules, both present in this solvent. This data lead us to think that the DMAc solvent was not properly evaporated from the microcomposite sample, in spite of the long time spent inside of an oven at 60°C used for all samples.
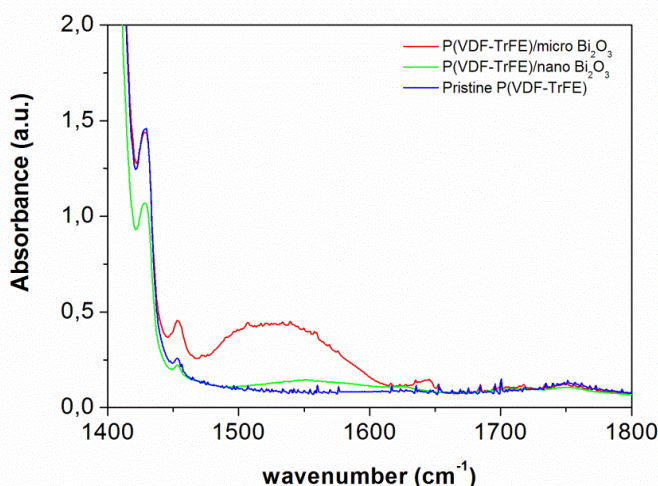
Figure 6: FTIR spectra of P(VDF-TrFE) copolymer and P(VDF-TrFE)/Bi$_2$O$_3$ nano and microcomposites for wavenumbers ranging from 1400 cm^{-1} to 1800 cm^{-1}.

Finally, we may now investigate the radiation shielding properties of these composites filled with Bi_2O_3 nano and micro particles. Bismuth has a huge mass attenuation coefficient (μ/ρ) for X-ray energies ranging from 5 keV to 100 keV. Its *μ/ρ x Photon Energy* relationship is equal to that of Lead, although it has a lower density (9.8 g/cm³). For this reason, conventional-sized Bismuth Oxide has been used in a bismuth-coated latex shields (340 g/cm²) for breast radiography for decades [12,13]. It is also the reason we decided to investigate nanocomposites filled with Bi_2O_3 for application in X-ray shielding.

In order to determine the radiation attenuation for monoenergetic photons we have exposed P(VDF-TrFE) and the nano and microcomposites with Bi_2O_3 to X-rays with energies of 6.5 keV, 17.5 keV and 22.1 keV using the setup depicted in **Figure 1**. The beam percentage attenuation (*At%*) is given by

$$At\% = \left(1 - \frac{I}{I_0}\right) x 100 \qquad (1)$$

where I_0 is the intensity of the X-ray beam on the frontal sample surface and I is the X-ray intensity of the attenuated beam. **Figure 7** displays the radiation percentage attenuation obtained for our samples. The thickness sample was normalized to 0.5 mm by using the Beer Lamber law.

$$\frac{I}{I_0} = e^{-\left(\frac{\mu}{\rho}\right)\rho x} \qquad (2)$$

where μ is the mass linear coefficient (cm⁻¹), ρ is the density (g/cm³) and x is the thickness (cm). The data for pristine P(VDF-TrFE) is absent, for energies 17.5 keV and 22.1 keV, because there was practically no attenuation. The sample thickness was too thin (30 μm) and the XRD NaI detector was not able to detect the very small difference between I and I_0. In this figure we observe that the percentage attenuation of P(VDF-TrFE)/nano Bi_2O_3 composite is larger than that of microcomposite in the energy range studied. For 6.5 keV photons, 65% of the X-ray beam was attenuated by the nanocomposite 0.5 mm thick.

Figure 8 displays the radiation percentage attenuation obtained for X-ray of non-monochromatic fields, irradiated at the same dose (100 mGy), for the X-ray beam qualities RQR2 (40 kV), RQR5 (70 kV) and RQR 8 (100 kV). The mean energy for these beams are 33 keV, 54 keV and 83.5 keV, respectively. The sample thickness has been normalized to 0.5 mm by using equation 2. For comparison purposes, the percentage attenuation of Bismuth, calculated using the table for the mass attenuation coefficient from NIST (National Institute of Standards and Technology) is also displayed. We note that percentage attenuation of P(VDF-TrFE)/nano Bi_2O_3 composite is again larger than that of microcomposite for the energy range studied. For the beam quality RQR 2 (40 kV, E_{mean}=33 keV), 41% of the X-ray beam was attenuated by the nanocomposite 0.5 mm thick.
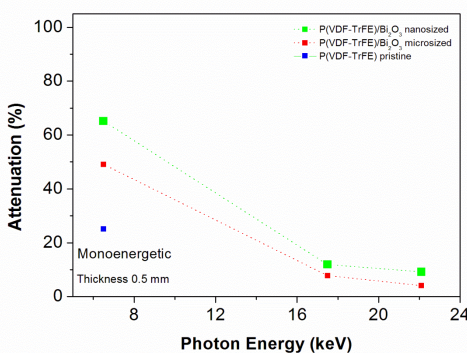
Figure 7: X-ray beam attenuation of P(VDF-TrFE) copolymer and P(VDF-TrFE)/Bi_2O_3 nano and microcomposites as a function for 6.6 keV, 17.5 keV and 22.1 keV monoenergetic photons. The thickness sample was normalized to 0.5 mm.
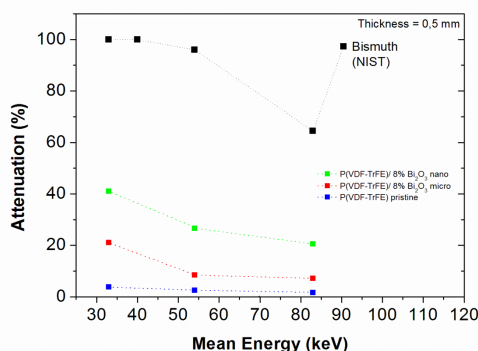
Figure 8: X-ray beam attenuation of P(VDF-TrFE) copolymer and P(VDF-TrFE)/Bi_2O_3 nano and microcomposites as a function for 33 keV, 54 keV and 83.5 keV mean energies of the X-ray beam qualities RQR2 (40 kV), RQR5 (70 kV) and RQR 8 (100 kV). The thickness sample was normalized to 0.5 mm

DISCUSSION

The first point to be discussed is the huge difference concerning to porosity observed in the SEM images **(Figure 3b and 3c**, right side) between the P(VDF-TrFE)/nano Bi_2O_3 and P(VDF-TrFE)/micro Bi_2O_3. The difference in porosity can be also observed in the SEM images obtained with higher magnification in **Figure 3a and 3b** (left side). We remark that both composites were produced using the same methodology. On the other hand, a very similar process of porosity formation has been reported to occur when casting PVDF homopolymer from DAMc solution, at temperatures below 80°C [21]. This methodology is similar to that used in this work. The authors argue that micro-pore formation occurs due to the evaporation rate of solvent, where, at lower annealing temperature, the evaporation rate of DMAc is slower and produces the pores. The analysis of FTIR data displayed in **Figure 6** suggests that the wide and large absorption band at 1530 cm^{-1} in the P(VDF-TrFE)/micro Bi_2O_3 composite spectrum is due to the presence of DMAc in the sample, once they can be associated to the C=O stretch (1635-1655 cm^{-1}) and to the CH_3 antisymetric deformation (1440-1470 cm^{-1}) molecules, both present in this solvent. This band is also present in the nanocomposite sample, but with a very lower intensity. Thus, as in this work evaporation is performed at 60°C, a possible explanation for the case of P(VDF-TrFE)/Bi_2O_3 composites is that the lower volume of the Bi_2O_3 nanoparticles, compared with microsized ones, could be linked to a lower decrease of the evaporation rate, decreasing the amount of pores. In this context, the evaporation rate in P(VDF-TrFE)/Bi_2O_3 microcomposites would be lower, leading to the presence of DMAc absorption bands observed in **Figure 6,** and increasing the pore formation observed in the SEM images in **Figure 3b and 3c**.

The second point to be discussed is related to the lack of the microsized Bi_2O_3 crystalline peaks in the P(VDF-TrFE)/Bi_2O_3 microcomposite diffractogram observed in **Figure 4b**, suggesting that, during the synthesis process, some kind of chemical reaction must have broken the microsized Bi_2O_3 crystalline arrangement. Here again we must look to the analysis of FTIR data and the SEM images. According to these analysis, the P(VDF-TrFE)/Bi_2O_3 microcomposite sample may contain DMAc traces and it is also full of pores. Taking into account that the nanocomposite samples do not present these anomalies, we think that they could be linked to the break of the microsized Bi_2O_3 crystalline arrangement.

Finally, we remark that the in the X-ray shielding characterization, once the amount of Bi_2O_3 in the composites is the same, we expected that the percentage of attenuation should be also the same. The data in **Figures 7 and 8** demonstrate that the nanocomposite has better attenuation properties than the microcomposite in the entire photon energy range studied. Here, it seems clear to us that the large presence of pores in the microcomposite has directly influenced its poor attenuation properties, when compared to the nanocomposites. Another interesting feature we would like to address is the percentage attenuation observed for the 83.5 keV mean energy beam, which is higher than expected. We think that the reason behind this behavior is that the mean energy is close to energy of the Bismuth k-shell (around 90.5 keV). In this sense, the 100 kV X-ray beam used also contains photons with energy ranging from 90 keV to 100 keV that have energy enough to eject the k-electrons. This causes an abrupt increase in the mass attenuation coefficient of Bismuth, provoking an increase in the percentage attenuation (seen in **Figure 8**). In other words, it acts as a radiation filter for photons with energy higher than 90 keV. In fact, in some interventional radiology X-ray machines, as for instances fluoroscopy and mammography, the manufacturers use the k-shell of Rh or Mo also for removing unwanted photon energies. Thus, the nanocomposites made of P(VDF-TrFE)/nano Bi_2O_3 are good candidates to be used particularly as breast shields in pediatric Computerized Tomography (CT scanning), which uses a 120 kVp X-ray beam, due to its ability of shielding unwanted photons with energy higher than 90 keV.

CONCLUSION

Nano and microcomposites made of P(VDF-TrFE) copolymers and nano and microsized Bi_2O_3 particles were synthetized and investigated for application in X-ray shielding. The bismuth oxide was previously surface-modified with methyl-methacrylate acid (MMA) in order to improve the homogeneity distribution. The X-ray shielding characterization was performed for photons with energies ranging from 6.5 keV to 83.5 keV. The nanocomposite P(VDF-TrFE)/nano Bi_2O_3-MMA revealed to have better attenuation features than the microcomposite, in the entire range of energy studied. DRX measurements confirm that the microsized Bi_2O_3 lost its crystalline structure inside the microcomposite. DSC, FTIR and SEM images data were used to explain the high degree of porosity present in the microcomposite, which in turn, was responsible for its worse radiation attenuation properties. For 6.5 keV photons, 65% of the X-ray beam was attenuated and for the beam quality RQR 2 (40 kV, E_{mean}=33 keV), 41% of the X-ray beam, both by the nanocomposite 0.5 mm thick. The investigation has demonstrated that the P(VDF-TrFE)/nano Bi_2O_3-MMA nanocomposites are good candidates for application in radiology procedures as lightweight, conformable, flexible, and easy to process X-ray shielding materials, and particularly as breast shields in pediatric Computerized Tomography.

ACKNOWLEDGEMENTS

REFERENCES

1. Miller DL, et al. Radiation Doses in Interventional Radiology Procedures: The RAD-IR Study Part I: Overall Measures of Dose. J Vasc Interv Radiology 2003; 14: 711–727.

2. Brambilla M, et al. Patient radiation doses and references levels in interventional radiology. Radiol Med 2004; 107: 408-418.

3. Nambiar S and Yeow JTW. Polymer-Composite Materials for Radiation Protection. ACS Appl Mater Interfaces 2012; 4: 5717–5726.

4. Zhang W, et al. A novel property of styrene–butadiene–styrene/clay nanocomposites: radiation resistance. J Mater Chem 2004; 14: 209–213.

5. Tiwari VK, et al. Nanoparticle induced piezoelectric, super toughened, radiation resistant, multi-functional nanohybrids. Nanoscale 2012; 4: 167-175.

6. Samarasmpm M, et al. Radiation damage near grain boundaries. Philos Mag 2003; 83: 3599–3607.

7. Chimi Y, et al. Accumulation and recovery of defects in ion-irradiated nanocrystalline gold. J Nucl Mater 2001: 297: 355–357.

8. Chimi Chimi Y, et al. Swift heavy ion irradiation effects in nanocrystalline gold. Nucl Instrum Methods Phys Res Sect B 2006; 245: 171–175.

9. Iqbal HMS, et al. Processing and characterization of space-durable high-performance polymeric nanocomposite. J Thermophys Heat Transfer 2011; 25: 87–95.

10. Bhowmik S and Benedictus R. IEEE Applied Electromagnetic Conference, Kolkata, India 2007.

11. Gaier JR, et al. Effect of Intercalation in Graphite Epoxy Composites on the Shielding of High Energy Radiation; NASA Technical Memorandum 107413, 1997 National Aeronautics and Space Administration: Washington, D.C., USA.

12. Hopper KD, et al. The breast: in-plane x-ray protection during diagnostic thoracic CT—shielding with bismuth radioprotective garments. Radiology 1997; 205: 853–858.

13. Fricke BL, et al. In-Plane Bismuth Breast Shields for Pediatric CT: Effects on Radiation Dose and Image Quality Using Experimental and Clinical Data. Am J Roentgenol 2003; 180: 407–411.

14. Nambiar S, et al. Polymer Nanocomposite-Based Shielding Against Diagnostic X-rays. J Appl Polym Sci 2013; 127: 4939-4946.

15. Prateek, et al. Recent progress on Ferroelectric Polymer-Based Nanocomposites for High Energy Density Capacitors: Synthesis, Dielectric Properties, and Future Aspects. Chem Rev 2016; 116: 4260-4317.

16. Kong LB, et al. Progress in Synthesis of Ferroelectric Ceramic Materials via High-Energy Mechanochemical Technique. Prog Mater Sci 2008; 53: 207–322.

17. Castro M, et al. Carbon Nanotubes/Poly(ε-caprolactone) Composite Vapour Sensors. Carbon 2009; 47: 1930–1942.

18. Fontainha CCP, et al. P(VDF-TrFE)/ZrO_2 Polymer-Composites for X-ray Shielding. Mat Res 2016; 19: 91-99.

19. Faria LO and Moreira RL. Infrared Spectroscopic Investigation of Chain Conformations and Interactions in P(VDF-TrFE)/PMMA Blends. J Polymer Sci: Part B: Polymer Phys 2000; 38: 34-40.

20. Lovinger AJ. Developments in Crystalline Polymers. Edited by Basset IDC (Applied Science) London: Chapter 5, 1982.

21. Abdullah IY, et al. Influence of Temperature on Crystalline Structure of Polyvinylidene Fluoride. Intern J Tech Res Appl 2015; 23: 46-50.